J Therm Anal Calorim (2013) 113:335–342
DOI 10.1007/s10973-013-3225-x

Effect of Fe^{3+} ions present in the structure of poly(acrylic acid)/montmorillonite composites on their thermal decomposition

Piotr Natkański · Piotr Kuśtrowski · Anna Białas · Janusz Surman

Received: 16 October 2012 / Accepted: 26 April 2013 / Published online: 21 May 2013

Abstract Poly(acrylic acid)/montmorillonite (MMT) composites with various polymer contents were synthesized by in situ polymerization technique. The structure of obtained materials was characterized by powder X-ray diffraction and infrared spectroscopy (FTIR). It was found that only a limited amount of hydrogel could be introduced between the clay layers. The remaining part of polymer was deposited on the external surface of clay particles. The introduction of the polymer modifier significantly increased the adsorption capacity of MMT in the elimination of Fe^{3+} ions from aqueous solution. The thermal behavior of the samples before and after the Fe^{3+} adsorption was examined by thermogravimetry and differential thermal analysis. Moreover, the composition of gaseous products evolved during decomposition was determined by FTIR. The materials after Fe^{3+} adsorption exhibited different thermal stability in oxidizing atmosphere than the fresh samples. Fe^{3+} cations, forming FeO_x species during thermal treatment, appeared to be effective catalysts of polymer oxidation.

Keywords Polymer–clay composites · Montmorillonite · Cation adsorption · Thermal stability

Introduction

Modification of clay structure has attracted great attention due to the possibility of obtaining promising materials to new applications. Various materials based on clay minerals, are extensively used in many fields of life and industry as nanocomposite fillers, thickeners in paints, oil-base drilling mud, adsorbents of heavy metals, and organic pollutants as well as catalysts (e.g., for Fischer–Tropsch synthesis, catalytic cracking, Friedel–Crafts reaction, combustion of volatile organic compounds, oxidation of H_2S) [1–10].

One of the most often investigated and abundant layered aluminosilicate is montmorillonite (MMT), belonging to the smectite group. In the MMT structure, the sheet containing Al^{3+} in octahedral coordination with O^{2-} and OH^- ions is sandwiched between two sheets with Si^{4+} in tetrahedral coordination with O^{2-} ions. The layers are interconnected by sharing O^{2-} at polyhedral corners and edges [11]. The partial substitution of Al^{3+} cations by lower valency ions (mainly Mg^{2+}) leads to the generation of negative charge on the clay layers, which is neutralized by hydrated, exchangeable cations (e.g., Ca^{2+}, Mg^{2+}, Na^+, K^+) located in the interlayer spaces. Such a structure causes that the interlamellar space of the natural clay can be functionalized through the replacement of interlayer ions by other species, for instance transition metal cations (or clusters), cationic surfactants, or monomers [12–15].

MMT can be used as a component of polymer–clay nanocomposites, which exhibit interesting functional and structural properties [16]. Superabsorbent composites are one group of such materials, in which the polymer matrix consists of hydrophilic polymers, mainly of poly(acrylic acid) (PAA) [17] and its salts [18], poly(acrylamide) [19, 20], 2-methylpropane sulfonic acid (AMPS), and their copolymers [21, 22]. These hybrid materials, due to their functional groups, are efficient adsorbents of heavy metals cations (e.g., Pb^{2+}, Cd^{2+}, Cu^{2+}) or dyes [22–24] often tested in water purification.

The aim of this article was the synthesis and characterization of PAA/MMT composites designed as metal adsorbents. The influence of hydrogel content in a composite on

P. Natkański · P. Kuśtrowski (✉) · A. Białas · J. Surman
Faculty of Chemistry, Jagiellonian University, Ingardena 3, 30-060 Kraków, Poland
e-mail: kustrows@chemia.uj.edu.pl

the Fe^{3+} adsorption capacity as well as the effect of the presence of iron species on the thermal stability of the synthesized materials were investigated. Since clays modified with Fe turned out to be active catalysts of various processes (e.g., selective reduction of NO with ammonia [25], oxidation of phenol [26], alkylation of arenes [27], and dehydrogenation of alkanes [28]), the hydrogel/clay composites with adsorbed Fe^{3+} are expected to be a novel type of catalyst precursors for the mentioned reactions. Therefore, investigation into their thermal behavior is crucial to optimize the conditions of calcination, which could result in obtaining Fe-doped aluminosilicate materials with highly dispersed transition metal oxide phase.

Experimental

Materials

Wyoming MMT with cation exchange capacity (CEC) of 90 meq/100 g and the chemical composition as follows: 47.8 % O, 32.3 % Si, 13.6 % Al, 2.5 % Fe, 1.9 % Mg, 0.9 % Na, 0.7 % Ca, 0.2 % K, was used to the synthesis. Acrylic acid (AA) was purchased from Arkema (France). Ammonium persulfate (APS) and *N*,*N*′-methylenebisacrylamide (MBA) were supplied by Sigma-Aldrich. Iron(III) nitrate nonahydrate and potassium thiocyanate, used in adsorption studies, were purchased from POCh (Poland).

Synthesis of composites

The series of PAA/MMT composites was prepared by in situ polymerization. The AA monomer was dissolved in deionized water to obtain 10 mass% solution. In the prepared solution, various amounts of clay were dispersed. MMT was introduced at MMT/AA mass ratios of 1.0, 1.5, 2.3, and 4.0. Subsequently, the MBA crosslinking agent was added at a MBA/monomer molar ratio of 0.01. The mixture was stirred at 400 rpm at room temperature to obtain homogenous suspension. The slurry was purged with argon for 10 min to remove oxygen and then the APS initiator (at a APS/monomer molar ratio of 0.01) was added. The mixture was heated to 338 K and kept at this temperature for 3 h until the complete polymerization of monomers. Such obtained material was cut to small pieces, dried at 333 K and ground to fine powder. The composites were denoted as MMT-PAA-20, MMT-PAA-30, MMT-PAA-40, and MMT-PAA-50, where the number indicates the polymer content in composite.

Methods

X-ray diffraction (XRD) analysis was performed by means of a Bruker D2 Phaser X-ray powder diffractometer (30 kV, 10 mA) with Cu anode ($\lambda = 0.15406$ nm) at room temperature. The patterns were collected in the 2θ range of 2–50° with step size of 0.02° and scan rate of 1 s.

The structure of composites and raw MMT was additionally investigated using a Thermo Scientific Nicolet 6700 FTIR spectrometer equipped with a DRIFT (EasyDiff) accessory and a MCT-A detector. The dried samples of clay and composites were ground with dried potassium bromide powder (10 mass%). FTIR spectra were recorded from 650 to 4,000 cm^{-1} collecting 200 scans with 2 cm^{-1} resolution.

The kinetics of Fe^{3+} cations adsorption from aqueous solution was examined in batch experiments. Each sample (1 g) was immersed in 300 mL of 0.01 M iron(III) nitrate solution. The solutions were stirred at 303 K for 27 h with an agitation rate of 200 rpm. During the adsorption tests, pH of a solution was maintained at 2.5 using 0.1 M HNO_3 and 0.1 M KOH. The changes in the metal ion concentration were determined by means of a Merck Spectroquant Pharo 100 VIS spectrophotometer using thiocyanate method with measurements of absorbance at $\lambda_{max} = 480$ nm. The amount of adsorbed metal ions was calculated from the following equation,

$$q_t = \frac{(C_0 - C_t)}{m} \cdot V$$

where q_t is the amount of Fe^{3+} cations adsorbed by a unit amount of composite after time t (mg g^{-1}), C_0 and C_t are the concentrations of Fe^{3+} ions in the initial solution before adsorption and after time t, respectively (mmol mL^{-1}), V is the volume of the solution containing Fe^{3+} cations (mL), and m is the mass of composite (g).

Thermal stability studies of dry samples before and after adsorption of Fe^{3+} ions were performed by means of a TA Instruments SDT Q600 thermoanalyzer in the temperature range of 303–1,273 K at a heating rate of 10 K min^{-1} using a dry air purge at a flow rate of 100 mL min^{-1} (or 20 mL min^{-1} in the case of TG–FTIR study). The initial sample mass was about 20 mg in each run. The FTIR spectral maps of evolving gaseous products were measured with a Nicolet 6700 FTIR (Thermo Scientific) spectrometer equipped with a FTIR–TG (Thermo Scientific) accessory. Spectra were recorded with 4 cm^{-1} resolution collecting 8 scans for each spectrum.

Results and discussion

Structure of PAA/montmorillonite composites

The structure of clay and PAA/clay composites was investigated by XRD. The XRD patterns are shown in the Fig. 1. The basal spacing in raw clay and composites was calculated according to the Bragg equation based on the

position of (001) diffraction peak. The (001) interplanar distance of raw MMT was 1.22 nm. After the modification with various amounts of PAA the lamellar structure of starting mineral was retained. Moreover, the (001) peak was shifted to the lower 2θ angles (5.08°–5.37°). This indicates an increase in the d_{001} spacing of the clay by about 0.43–0.52 nm. For the MMT-PAA-20 sample containing the lowest amount of polymer, the d_{001} spacing increased to a lesser degree (1.64 nm) compared to other composites, which resulted from the intercalation of the lower amount of polymer into the interlayer space. In the case of the materials with higher content of PAA, the differences in the distance between the layers slightly varied (in the range of 1.72–1.74 nm). Thus, one can conclude that only limited amount of hydrogel can be intercalated into the interlayer gallery of MMT. The remaining part of polymer probably forms on the external surface of MMT particles.

The deeper insight into the structure of MMT and PAA/clay composites was possible due to FTIR measurements. The FTIR spectra of these materials are presented in Fig. 2. In the spectrum of MMT, characteristic absorption peak of hydroxyl group bound with Al^{3+} cations is observed at 3,630 cm^{-1}. The stretching and bending vibrations of the hydroxyl groups of water molecules present in the clay can be noticed at 3,430 and 1,645 cm^{-1}, respectively. The most intensive band at 1,015 cm^{-1} is attributed to Si–O in-plane stretching, while the shoulder at 1,115 cm^{-1} comes from Si–O out-of-plane stretching vibrations. The three peaks below 1,000 cm^{-1} originate from bending vibrations of Al–Al–OH (920 cm^{-1}), Al–Fe–OH (887 cm^{-1}), and Al–Mg–OH (844 cm^{-1}). Furthermore, Si–O stretching of SiO_2 admixture phase (most probably quartz detected by XRD) appears at 798 cm^{-1} [29].

Beside the characteristic bands of MMT, absorption bands attributed to the PAA part are found in the FTIR spectra of composites. The peaks at 2,945–2,950 cm^{-1} (CH_2 stretching), 1,453 cm^{-1} (CH_2 deformation), and 1,316 cm^{-1} (C–C stretching) are associated with a carbon backbone chain. Other three distinct peaks at 1,717, 1,540, and 1,410 cm^{-1} can be assigned to the C=O stretching mode in the protonated carboxylate group as well as to the asymmetric and symmetric C–O stretching modes in the COO^- ions, respectively [30]. For all the composites, the wide absorption band observed between 2,700 and 3,500 cm^{-1} indicates a significant amount of absorbed water. The presence of undissociated COOH groups is confirmed by the maximum between 2,500 and 2,600 cm^{-1}, attributed to hydrogen bonds involving polymeric species [31].

Simultaneous thermogravimetric (TG) and differential thermal analyses (DTA) were performed in order to study the mechanism of thermal decomposition of the polymer part present in the MMT structure. In the case of the MMT sample, only two mass loss effects are observed. The first one (up to 433 K) is attributed to the dehydration of the material and the next one (above 823 K) to dehydroxylation of MMT layers. The results obtained for the MMT-PAA composites are presented in Fig. 3. As seen, the physically adsorbed and interlayer water was removed to 443 K. Above this temperature, the complex decomposition of organic matrix is observed. At first, the carboxyl side groups underwent decomposition to 588–600 K which

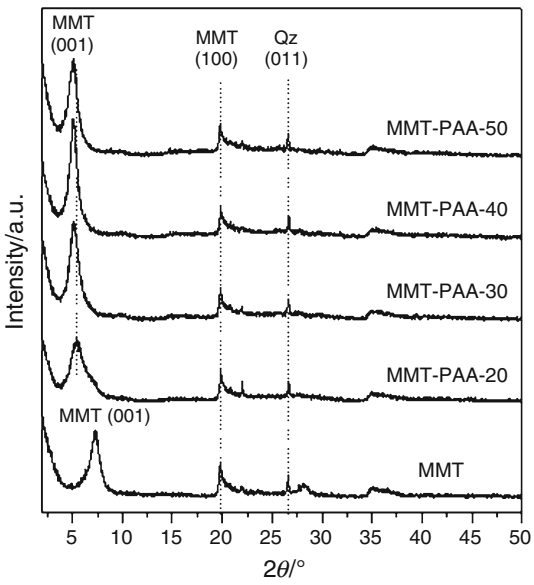

Fig. 1 XRD patterns of raw montmorillonite and the series of poly(acrylic acid)/montmorillonite composites

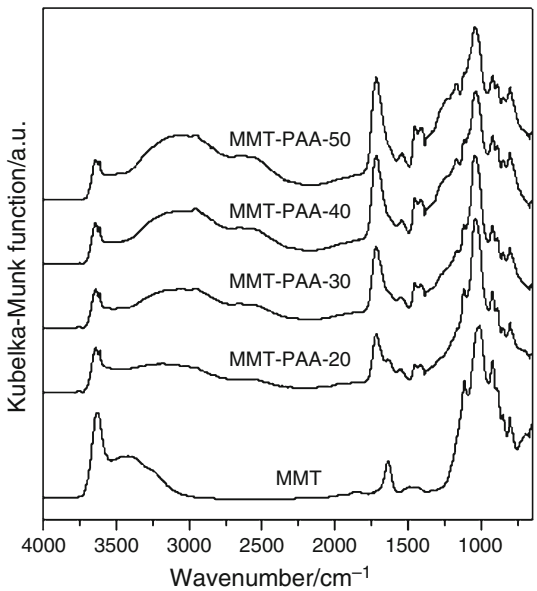

Fig. 2 DRIFT spectra of clay and PAA/MMT composites

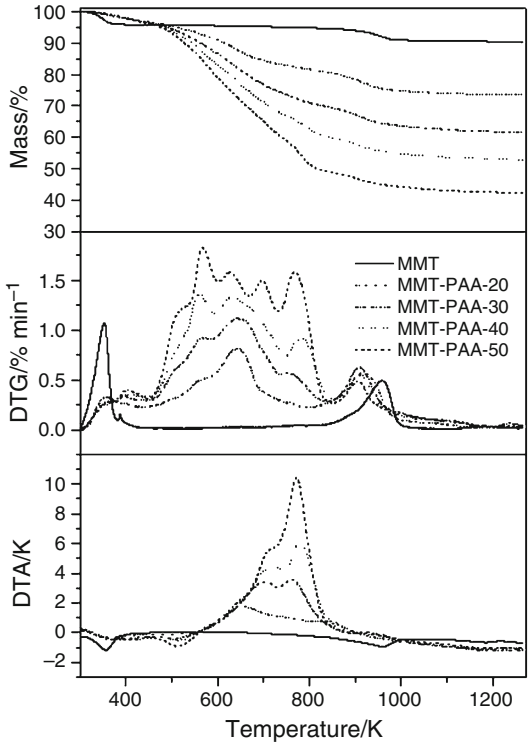

Fig. 3 TG, DTG, and DTA curves recorded for raw montmorillonite and the series of PAA/MMT composites before Fe^{3+} ions adsorption

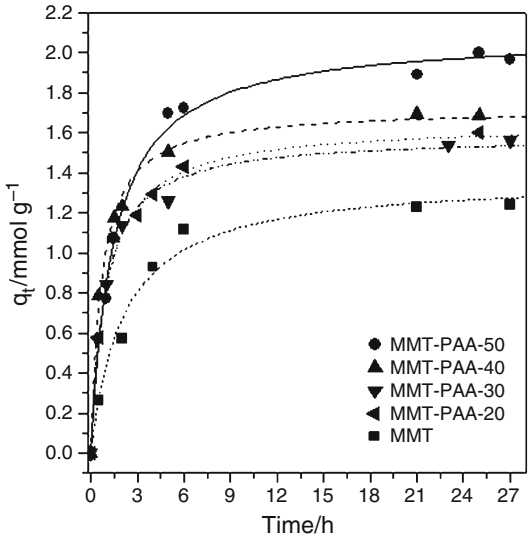

Fig. 4 Adsorption kinetics of Fe^{3+} ions for raw montmorillonite and composites

was detected in the DTG curves as mass loss effects and in the DTA curves as endothermic peaks. A further increase in temperature resulted in oxidation of carbon backbone chains, confirmed by two step exothermic maximum in the temperature range of 600–900 K [20]. Above 900 K, the dehydroxylation of MMT was observed. The evaluated mass losses attributed to the polymer part in composites (compared in Table 1) are close to the intended values.

Adsorption capacity of PAA/montmorillonite

The efficiency of raw MMT and composites in the adsorption of Fe^{3+} cations from aqueous solution was studied. Adsorption kinetics was examined to determine the adsorption capacity and to explain the adsorption mechanism. The experimental data were fitted using the pseudo-first-order kinetic equation [32]:

$$\ln(q_e - q_t) = \ln q_e - k_f t$$

where k_f is the adsorption rate constant for the first-order adsorption, q_t (mmol g^{-1}) is the amount of Fe^{3+} cations adsorbed at time t, and q_e (mmol g^{-1}) is the amount of Fe^{3+} ions adsorbed at equilibrium; and pseudo-second-order kinetic equation [33]:

$$\frac{t}{q_t} = \frac{1}{k_s {q_e}^2} + \frac{t}{q_e}$$

where k_s is the adsorption rate constant for the second-order adsorption.

The experimental q_t values collected during the measurements are presented in Fig. 4, and the calculated kinetic parameters are collected in Table 1. The kinetic results of adsorption of Fe^{3+} ions suggest that in the case of composite materials the adsorption occurred according to the model of pseudo-second-order, whereas for the MMT sample the pseudo-first-order kinetic model describes better this process. It can be noticed that an increase in the

Table 1 Comparison of adsorption parameters of the raw montmorillonite and the PAA/MMT composites

Sample	Polymer content/mass%	Pseudo-first-order kinetic model			Pseudo-second-order kinetic model		
		k_f/h^{-1}	q_e/mmol g^{-1}	R_1^2	k_s/g mmol^{-1} h^{-1}	q_e/mmol g^{-1}	R_2^2
MMT	–	0.346	1.24	0.995	0.339	1.38	0.985
MMT-PAA-20	18.9	0.646	1.48	0.976	0.599	1.64	0.998
MMT-PAA-30	28.9	0.765	1.47	0.972	0.713	1.58	0.994
MMT-PAA-40	38.7	0.928	1.61	0.968	0.857	1.72	0.997
MMT-PAA-50	48.6	0.533	1.91	0.990	0.332	2.09	0.995

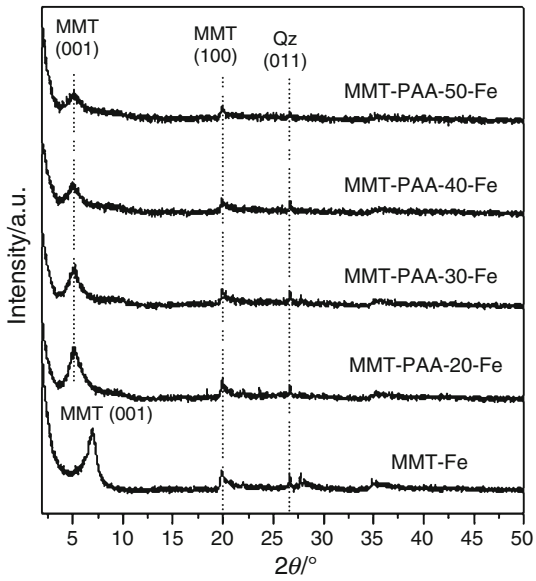

Fig. 5 XRD patterns of raw montmorillonite and the series of poly(acrylic acid)/montmorillonite composites after Fe^{3+} cations adsorption

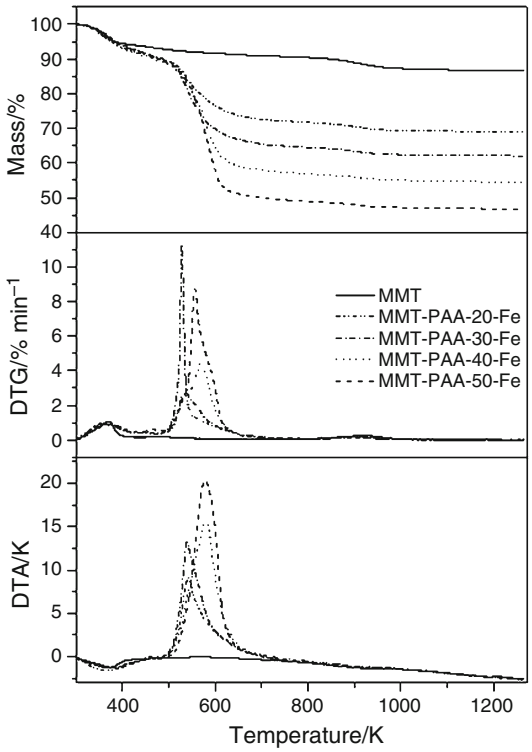

Fig. 6 TG, DTG, and DTA curves recorded for the series of PAA/MMT composites and montmorillonite containing Fe^{3+} cations

Table 2 Position of d_{001} diffraction peak and basal spacing of the clay and the PAA/MMT composites before and after adsorption of Fe^{3+} ions as well as amounts of Fe^{3+} ions eliminated by adsorption

Sample	Amount of adsorbed Fe^{3+} cations/mg g^{-1}	Structural properties			
		Before Fe^{3+} sorption		After Fe^{3+} sorption	
		Position of d_{001} line/°2θ	d_{001} spacing/nm	Position of d_{001} line/°2θ	d_{001} spacing/nm
MMT	69.3	7.26	1.22	6.95	1.27
MMT-PAA-20	91.6	5.37	1.64	5.11	1.73
MMT-PAA-30	88.2	5.13	1.72	5.07	1.74
MMT-PAA-40	96.1	5.10	1.73	5.02	1.76
MMT-PAA-50	116.7	5.08	1.74	4.99	1.77

content of PAA in composite has a positive impact on the adsorption capacity of Fe^{3+} cations. This effect can be attributed to the high efficiency of carboxyl groups in the adsorption of Fe^{3+} cations by ion exchange with protons.

Structural characterization and thermal stability of PAA/montmorillonite composites after Fe^{3+} adsorption

The structure of the studied materials after adsorption of Fe^{3+} cations was examined using XRD analysis. The diffraction patterns of the clay and the composite materials containing Fe^{3+} ions are presented in Fig. 5. The position of main (001) diffraction peak and basal spacing (d_{001}) for all examined materials before and after the adsorption of Fe^{3+} cations as well as amounts of adsorbed metal ions are presented in Table 2. The Fe^{3+} ions' content in samples was calculated based on the results of adsorption experiments. After adsorption the insignificant changes in the d_{001} spacing of all materials were observed which resulted from the introduction of metal ions into the interlayer spaces. Furthermore, a decrease in the intensity of (001) diffraction line was the result of partial delamination of clay structure caused by adsorption of Fe^{3+} cations between aluminosilicate layers.

The effect of Fe^{3+} ions present in the structure of PAA/MMT composites on the mechanism of their thermal decomposition was studied using thermal analysis techniques. The TG, DTG, and DTA curves recorded for the composite materials with adsorbed Fe^{3+} cations are presented in Fig. 6. The example results of TG–FTIR experiments, testing thermal decomposition of the MMT-PAA-30 sample before and after adsorption of Fe^{3+} cations, are shown in Fig. 7.

In the case of the iron-free material, the elimination of carboxyl groups in the temperature range of 460–640 K was the first step of PAA decomposition. It was confirmed by two peaks at 1,765 and 1,136 cm^{-1} attributed to vibrations of C=O and C–O bonds, respectively [34]. From 505 to 1,030 K, two intensive and wide bands (at 2,250–2,400 and 670–750 cm^{-1}) originating from carbon

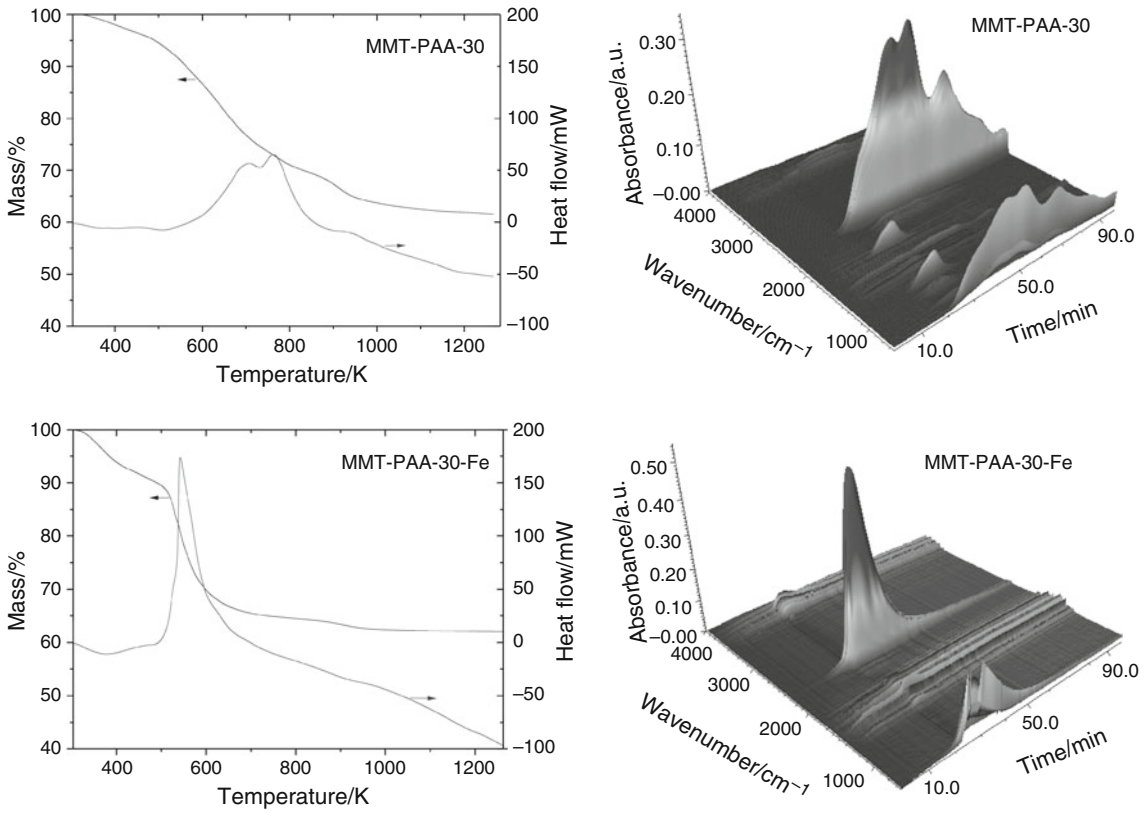

Fig. 7 TG–FTIR results for MMT-PAA-30 composite before and after adsorption of Fe^{3+} cations

dioxide indicate the combustion of carbon backbone. In this temperature range, three exothermic maxima are observed on the DTA curves. The first peak (505–720 K) is most likely connected with the thermal decomposition of polymer deposited on external surface of clay particles, while the second effect (735–890 K) is related to the oxidation of polymer located in the interlayer spaces. The last low intensive peak (above 890 K) can be attributed to the removal of carbon deposit formed between layers during the incomplete oxidation of hydrogel. The formation of the carbon deposit is confirmed by characteristic bands of carbon monoxide observed on the FTIR maps at 2,110–2,220 cm^{-1} in the temperature range of 596–968 K. Moreover, this last stage of the polymer decomposition overlaps with the dehydroxylation process starting at 900 K. The bands in the wavenumber ranges of 3,400–3,750 and 1,250–2,000 cm^{-1}, attributed to water formed during the oxidation of hydrogel, are observed in the temperature range of 500–1,010 K.

For the material after Fe^{3+} adsorption, the starting temperature of the thermal decomposition of polymer matrix did not change, however the temperature range of this process is narrower—from 443 to 760 K. Moreover, in the DTA curve only one exothermic peak is visible, which indicates fast oxidation of organic matrix. The gaseous products of this process formed in the temperature ranges of 533–673 and 505–795 K were water and carbon dioxide, respectively. The position of the maximum of this exothermic effect is different and depends on the PAA content and its location in the composite structure. In the case of the composites containing to 30 mass% of PAA, the Fe^{3+} cations are mainly adsorbed by hydrogel introduced between clay layers. In this case, the high concentration of Fe^{3+} in the interlayer gallery causes that during thermal treatment Fe^{3+} oxide particles are easily formed, which catalyze the oxidation of polymer. For the composites with 40 and 50 mass% of PAA, the decomposition temperature of hydrogel part is 30–35 K higher than for other materials. This effect can be explained by higher dispersion of adsorbed Fe^{3+} cations in PAA deposited on both external and internal surface of MMT. Thus, the formation of Fe oxide species, responsible for faster polymer oxidation, requires higher temperature than for the MMT-rich composites.

Conclusions

PAA can be introduced into the MMT structure by in situ polymerization. Only limited amount of PAA is

intercalated between the clay layers. The excess of the formed polymer is deposited on the external surface of the clay particles. PAA/MMT composites are effective adsorbents of metal cations from aqueous solution. The modification of the MMT structure with hydrogel significantly increases the adsorption capacity of Fe^{3+} ions. The adsorbed metal cations strongly influence the thermal stability of the composite. During heating, iron oxide species form, which catalyze the oxidation of polymer and it is decomposed much faster than in the iron-free material. Therefore, for complete transformation of PAA/MMT composite into a final oxide-type catalyst, thermal treatment at a temperature even below 700 K can be considered.

Acknowledgments This study was supported by the Polish National Science Centre under the Grant No. N N507 217640, and by the European Regional Development Fund in the framework of the Polish Innovation Economy Operational Program (Contract No. POIG.02.01.00-12-023/08), which financed the purchase of research equipment. Piotr Natkański wishes to thank for the financial support from DOCTUS scholarship co-founded by the European Social Fund.

References

1. Lapides I, Borisover M, Yariv S. Thermal analysis of hexadecyltrimethylammonium–montmorillonites. J Therm Anal Calorim. 2011;105:921–9.
2. de Paiva LB, Morales AR, Valenzuela Díaz FR. Organoclays: properties, preparation and applications. Appl Clay Sci. 2008;42:8–24.
3. Wang G-W, Hao Q-Q, Liu Z-T, Liu Z-W. Fischer–Tropsch synthesis over Co/montmorillonite—insights into the role of interlayer exchangeable cations. Appl Catal A. 2011;405:45–54.
4. Mills GA, Holmes J, Cornelius EE. Acid activation of some bentonite clay. J Phys Chem. 1950;54:1170–85.
5. Kloprogge JT, Duong LV, Frost RL. A review of the synthesis and characterization of pillared clays and related porous materials for cracking of vegetable oils to produce biofuels. Environ Geol. 2005;47:967–81.
6. Phukan A, Ganguli JN, Dutta DK. $ZnCl_2$-Zn^{2+}-montmorillonite composite: efficient solid acid catalyst for benzylation of benzene. J Mol Catal A. 2003;202:279–87.
7. Özcelik Z, Soylu GSP, Boz I. Catalytic combustion of toluene over Mn, Fe and Co-exchanged clinoptilolite support. Chem Eng J. 2009;155:94–100.
8. Chen M, Fan L, Qi L, Luo X, Zhou R, Zheng X. The catalytic combustion of VOCs over copper catalysts supported on cerium-modified and zirconium-pillared montmorillonite. Catal Comm. 2009;10:838–41.
9. Nogueira FGE, Lopes JH, Silva AC, Lago RM, Fabris JD, Oliveira LCA. Catalysts based on clay and iron oxide for oxidation of toluene. Appl Clay Sci. 2011;51:385–9.
10. Bineesh KV, Kim SY, Jermy BR, Park DW. Synthesis, characterization and catalytic performance of vanadia-doped delaminated zirconia-pillared montmorillonite clay for the selective catalytic oxidation of hydrogen sulfide. J Mol Catal A. 2009;308:150–8.
11. Tyagi B, Chudasama CD, Jasra RV. Determination of structural modification in acid activated montmorillonite clay by FT-IR spectroscopy. Spectrochim Acta A. 2006;64:273–8.
12. Bia G, De Pauli CR, Borgnino L. The role of Fe(III) modified montmorillonite on fluoride mobility: adsorption experiments and competition with phosphate. J Environ Manag. 2012;100:1–9.
13. Malla PB, Ravindranathan P, Kornarneni S, Roy R. Intercalation of copper metal clusters in montmorillonite. Nature. 1991;351:555–7.
14. Janovák L, Varg J, Kemény L, Dékány I. Swelling properties of copolymer hydrogels in the presence of montmorillonite and alkylammonium montmorillonite. Appl Clay Sci. 2009;43:260–70.
15. Sinha Ray S, Okamoto M. Polymer/layered silicate nanocomposites: a review from preparation to processing. Prog Polym Sci. 2003;28:1539–641.
16. Pinnavaia TJ, Beall AG. Polymer-clay nanocomposites. New York: Wiley; 2002.
17. Molu ZB, Seki Y, Yurdakoc K. Preparation and characterization of poly(acrylic acid)/pillared clay superabsorbent composite. Polym Bull. 2010;64:171–83.
18. Santiago F, Mucientes AE, Osorio M, Rivera C. Preparation of composites and nanocomposites based on bentonite and poly(-sodium acrylate). Effect of amount of bentonite on the swelling behavior. Eur Polym J. 2007;4:1–9.
19. Helvacıoğlu E, Aydın V, Nugay T, Nugay N, Uluocak BG, Şen S. High strength poly(acrylamide)-clay hydrogels. J Polym Res. 2011;18:2341–50.
20. Zhang J, Wang A. Study on superabsorbent composites. IX: synthesis, characterization and swelling behaviors of polyacrylamide/clay composites based on various clays. React Funct Polym. 2007;67:737–45.
21. Zhou M, Zhao J, Zhou L. Utilization of starch and montmorillonite for the preparation of superabsorbent nanocomposite. Appl Polym Sci. 2011;121:2406–12.
22. Kaşgöz H, Durmuş A, Kaşgöz A. Enhanced swelling and adsorption properties of AAm-AMPSNa/clay hydrogel nanocomposites for heavy metal ion removal. Polym Adv Technol. 2008;19:213–20.
23. Bulut Y, Akçay G, Elma D, Serhatlı IE. Synthesis of clay-based superabsorbent composite and its sorption capability. J Hazard Mater. 2009;171:717–23.
24. Kaplan M, Kasgoz H. Hydrogel nanocomposite sorbents for removal of basic dyes. Polym Bull. 2011;67:1153–68.
25. Chmielarz L, Kuśtrowski P, Dziembaj R, Cool P, Vansant EF. Selective catalytic reduction of NO with ammonia over porous clay heterostructures modified with copper and iron species. Catal Today. 2007;119:181–6.
26. Carriazo JG, Molina R, Moreno S. A study on Al and Al–Ce–Fe pillaring species and their catalytic potential as they are supported on a bentonite. Appl Catal A. 2008;334:168–72.
27. Sathyamoorthy A, Raj P, Gupta NM, Samant SD. Effect of preparation conditions on the characteristics of Fe^{3+}–K10 clay catalysts. Catal Lett. 2002;81:97–100.
28. Perez G, De Stefanis A, Tomlinson AAG. Pillared layered structures vs. zeolites as sorbents and catalysts Part 3. Comparison between some alumina-PILCs in ethylbenzene conversions to diethylbenzene and to styrene. J Mater Chem. 1997;7:351–6.
29. Sposito G, Prost R, Gaultier JP. Infrared spectroscopic study of adsorbed water on reduced-charge Na/Li-montmorillonites. Clay Clay Miner. 1983;31:9–16.

30. Kirwan LJ, Fawell PD, van Bronswijk W. In Situ FTIR–ATR examination of poly(acrylic acid) adsorbed onto hematite at low pH. Langmuir. 2003;19:5802–7.
31. Daniliuc L, David C. Intermolecular interactions in blends of poly(vinyl alcohol) with poly(acrylic acid): 2. Correlation between the states of sorbed water and the interactions in homopolymers and their blends. Polymer. 1996;37:5219–27.
32. Ho YS. Citation review of Lagergren kinetic rate equation on adsorption reactions. Scientometrics. 2004;59:171–7.
33. Ho YS, Mckay G. Batch lead (II) removal from aqueous solution by peat: equilibrium and kinetics. Trans Inst Chem Eng. 1999;77B:165–73.
34. Dong Y, Gui Z, Hu Y, Wu Y, Jiang S. The influence of titanate nanotube on the improved thermal properties and the smoke suppression in poly(methyl methacrylate). J Hazard Mater. 2012;209–210:34–9.